Electrochimica Acta 369 (2021) 137656

Contents lists available at ScienceDirect

Electrochimica Acta

journal homepage: www.elsevier.com/locate/electacta

Electropolymerization of [2 × 2] grid-type cobalt(II) complex with thiophene substituted dihydrazone ligand ☆

Sergiusz Napierała, Maciej Kubicki, Violetta Patroniak*, Monika Wałęsa-Chorab*

Faculty of Chemistry, Adam Mickiewicz University in Poznań, Uniwersytetu Poznańskiego 8, Poznań 61-614, Poland

ARTICLE INFO

Article history:
Received 4 September 2020
Revised 14 December 2020
Accepted 18 December 2020
Available online 30 December 2020

Keywords:
Grid-type complex
Cobalt(II)
Electrochromism
Thiophene
Electropolymerization

ABSTRACT

The grid-type complex $[Co_4(\mathbf{L1}\text{-}2H)_4]$ containing dihydrazone ligand decorated with thiophene rings has been prepared. The complex undergoes oxidative electropolymerization onto ITO electrode to form purple thin film. The morphology of polymer film on ITO electrode was analyzed by SEM and AFM imagining. It was found that polymer obtained by electropolymerization method is homogenous and uniform. The obtained thin film exhibits color transition from purple via violet to blue due to the stepwise reduction of **poly-**$[Co^{II}_4(\mathbf{L1}\text{-}2H)_4]$ into **poly-**$[Co^{II}_2Co^{I}_2(\mathbf{L1}\text{-}2H)_4]^{2-}$ and **poly-**$[Co^{I}_4(\mathbf{L1}\text{-}2H)_4]^{4-}$. Its electrochromic properties such as long-term stability coloration efficiency and switching times have been investigated.

1. Introduction

Grid-type complexes are architectures in which ligands and metal ions form a rectangular or square array and in which ligands that form nodes are crossed [1]. It has been shown that grid-type complexes can be deposited on surfaces to give ordered 2D supramolecular arrangements, where single grid units are addressable within the nanometer regime [2, 3]. Most of the self-assembled grid-type complexes reported to date contain metal ions of tetrahedral or octahedral coordination geometry, and examples of square [n × n] or rectangular [n × m] grids are well documented [4–9]. They are known to exhibit interesting chemical and physical properties, for example multielectron stable and reversible redox potentials in the cyclic voltammogram (CV), [10–12] Fe(II) and Co(II) grids show multistep spin-crossover (SCO) behavior [13–16] and lanthanide grid-like entities show single-molecule magnet (SMM) behavior [17, 18].

Transition metal complexes are attracting much attention due to their application as active materials in organic electronics. [19–22] Well defined redox properties and intense charge transfer absorption of transition metal complexes make them promising materials for their use as electrochromic materials. The major part of transition metal complexes examined as electrochromic materials are complexes with oligopyridines [23, 24] or phtalocyjanines, [25, 26] while electrochromic properties of transition metal complexes with Schiff base ligands and hydrazones have not been widely investigated [27].

Electropolymerization was found to be effective method in formation of thin films of materials [28–30]. Thiophene, [31–34] selenophene [35] and EDOT [26] groups have been used for formation of thin films of polymeric complexes. These groups are known to undergo oxidative electropolymerization when positive voltage is applied to the electrode and obtained in this way thin films have good adhesion and electrical contact to the electrode surface. Besides electropolymerization, the electrochromic polymers containing metals can be obtained as a self-assembled coordination polymers and sheets, [36–38] by coordinative layer-by-layer assembly [39, 40] or thermal polymerization [41]. The color change of electrochromic materials containing metal ions may be caused by a redox reaction of the metal ion and/or the ligand molecule when the complex contains the electrochromic ligand [42, 43]. Due to the electronic transitions that occur in polymeric complexes of transition metal ions which can be classified *i.a.* as d-d transitions, metal-to-ligand (MLCT) or ligand-to-metal (LMCT) charge transfers such materials exhibit interesting electrochromic properties [44–50]. As it is known that polynuclear character of monomers retains after polymerization and corresponding polymers exhibit similar electrochemical properties as the monomers from which they are built, and such materials can exhibit multielectrochromic properties, [43] we designed and prepared two grid-type complexes of cobalt(II) ions with $(N_2O)_2$-donor ligands **L1** and **L2** (Fig. 1).

One of the complexes is decorated with thiophene rings which are able to electropolymerization onto electrode surface. It was found the complex containing ligand **L1** undergoes the oxidative

☆ Dedicated to Professor Janusz Jurczak on his 80th birthday.

* Corresponding authors.
E-mail address: mchorab@amu.edu.pl (M. Wałęsa-Chorab).

https://doi.org/10.1016/j.electacta.2020.137656
0013-4686/

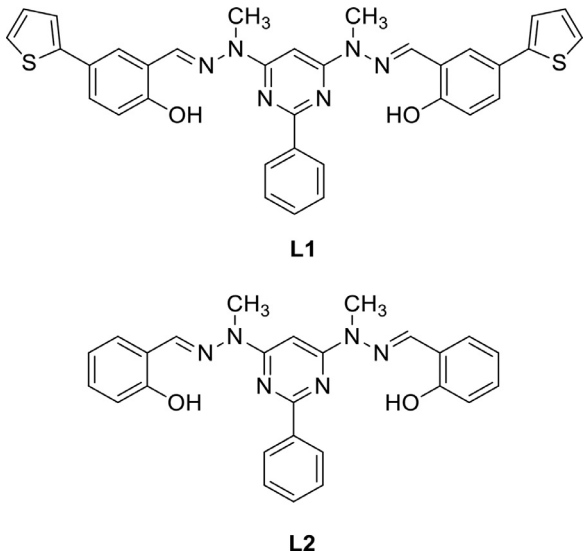

Fig. 1. Structures of ligands **L1** and **L2**.

electropolymerization during multi-scan cyclic voltammetry and it is the first example of electropolymerized grid-type complex. The electrochromic properties of the thin film have been investigated.

2. Experimantal section

Diffraction data were collected by the ω-scan technique at 130(1) K on Agilent Technologies SuperNova four-circle diffractometer with Atlas CCD detector and mirror-monochromated CuK$_\alpha$ radiation (λ=1.54178 Å. The data were corrected for Lorentz-polarization as well as for absorption effects [51]. Precise unit-cell parameters were determined by a least-squares fit of 3307 reflections of the highest intensity, chosen from the whole experiment. The structures were solved with SHELXT-2013 [52] and refined with the full-matrix least-squares procedure on F^2 by SHELXL-2013 [53]. All non-hydrogen atoms were refined anisotropically, hydrogen atoms were placed in idealized positions and refined as 'riding model' with isotropic displacement parameters set at 1.2 (1.5 for methyl or hydroxyl groups) times U_{eq} of appropriate carrier atoms.

Crystal data **2**: $C_{104}H_{88}Co_4N_{24}O_8$, M_r= 2037.70, tetragonal, $I4_1a$, a = 20.7736(3) Å, c = 23.3695(3) Å, V = 10084.9(3) Å^3, Z = 4, d_x= 1.342 g·cm^{-3}, μ = 5.616 mm^{-1}, F(000) = 4208. 16087 reflections collected up to 2Θ = 151.2°, 5119 symmetry independent (R_{int}= 2.29%), 4517 with I>2σ(I). Final R [I>2σ(I)] = 11.213.74%, wR2 [I>2σ(I)] = 10.98%, R [all refl.] = 4.37%, wR2 [all refl.] = 11.45%, S = 1.01, max/min $\Delta\rho$ = 0.22/-0.36 e·Å·$^{-3}$.

General: Reagents were used without further purification as supplied from Aldrich or Fluorochem. NMR spectra were run on a Brucker Ultra 300 MHz or Varian 400MHz spectrometer and were calibrated against the residual protonated solvent signals ($CDCl_3$, δ 7.24, DMSO 2.50 ppm) and shifts are given in parts per million. HRMS spectra were recorded on a QTOF mass spectrometer (Impact HD, Brucker) in positive ion mode. ESI mass spectra for acetonitrile solutions ~10^{-4} M of complexes were measured using a Waters Micromass ZQ spectrometer. Microanalyses were obtained using a Vario EL III CHN element analyzer. SEM and AFM images were done on the scanning electron microscope Quanta 250 FEG, FEI. XPS spectra were measured using a Specs UHV/XPS/SPM system. Al Kα was used as X-ray source. The sample of complex **1** was measured after deposition on a piece of a conducting carbon tape, while polymer **poly-1** was measured as prepared by electropolymerization on ITO-coated glass slide. The spectra were analysed using CasaXPS software and the binding energies were standardized using C 1s peak at 285.0 eV.

Electrochemical measurements were done using a multichannel BioLogic VSP potentiostat using anhydrous 0.1M solution of tetrabutylammonium perchlorate ($TBAClO_4$) in propylene carbonate (PC) as a supporting electrolyte. The investigated compounds were dissolved in electrolyte and the solutions were purged with argon for 20 min to remove the dissolved oxygen. A platinum electrode was used as a working electrode, platinum wire as a as the auxiliary electrode and the non-aqueous Ag/Ag$^+$ electrode as a reference electrode. Spectroelectrochemical measurements were done using a multi-channel BioLogic VSP potentiostat connected to a Jasco V-770 UV-vis-NIR spectrometer. ITO plate coated with the layer of **poly-1** was used as the working electrode with a platinum wire as the auxiliary electrode and the silver wire as a pseudoreference electrode. Before polymerization, ITO plates were cleaned by the sonication in water for 15 min, followed by the sonication in 2-propanol for 15 min, dried and cleaned by ozone generation using the Ossila UV-ozone cleaner.

3. Results and discussion

The ligands **L1** containing thiophene substituents has been synthesized in multistep synthesis as outlined in Fig. 2.

5-(thiophen-2-yl)salicylaldehyde **A** has been obtained in Suzuki-Miyaura coupling reaction between 5-bromosalicylaldehyde and 2-thienylboronic acid. The reaction was carried out in degassed THF/water mixture (3:1 v/v) under an argon atmosphere using potassium carbonate as a base, tetrakis(triphenylphosphine)palladium(0) as a catalyst and tetrabutylammonium bromide as a phase-transfer catalyst. In such conditions, the compound **A** has been obtained in high yield of 83%. In comparison, while using toluene/water mixture as a solvent, no reaction has been observed. It was probably due to the low solubility of 2-thienylboronic acid in toluene. 4,6-bis(1-methylhydrazinyl)-2-phenylpyrimidine **D** has been obtained according the method reported previously [54] starting from benzamidine hydrochloride and diethyl malonate (Figure S1), which in the malonic ester synthesis in the presence of sodium ethoxide gave 2-phenylpyrimidine-4,6-diol **B**. 4,6-Dichloro-2-phenylpyrimidine **C** has been obtained in the reaction of **B** with phosphoryl chloride followed by the reaction with methylhydrazine. Finally, the condensation of 4,6-bis(1-methylhydrazinyl)-2-phenylpyrimidine **D** with twofold molar amount of thiophene-substituted salicylaldehyde **A** carried out in absolute ethanol at 60°C for 24 h under an argon atmosphere gave ligand **L1** as a yellowish powder, which has been characterized by spectroscopic methods. Ligand **L1** has been further subjected to complexation reactions with cobalt(II) perchlorate. The reaction was carried out in 1:1 molar ratio in dichloromethane/acetonitrile (1:1 v/v) mixture for 48 h at room temperature. During the reaction, the precipitation of complex of Co(II) **1** occurred and it was isolated by centrifugation followed by washing with dichloromethane and diethyl ether. The complex has been characterized by spectroscopic methods and elemental analysis that confirmed 1:1 metal:ligand stoichiometry in obtained complexes. Due to the variety of supramolecular structures that can be formed in complexation reactions of transition metal ions with pyrimidine-dihydrazone based ligands [55, 56] unequivocal evidence of the structure of obtained compounds can be sought by X-ray crystallography. Due to the low solubility of obtained complex in common organic solvents it was impossible to obtain single crystal of **1** that could be suitable for the X-ray measurements. Due to this, we attempt to prepare ligand **L2** (Fig. S2), [57] being analogue of **L1**, which possess exactly the same structure and coordination donor subunits as **L1,** but its complexes are better soluble in organic solvents, such as acetonitrile, what makes

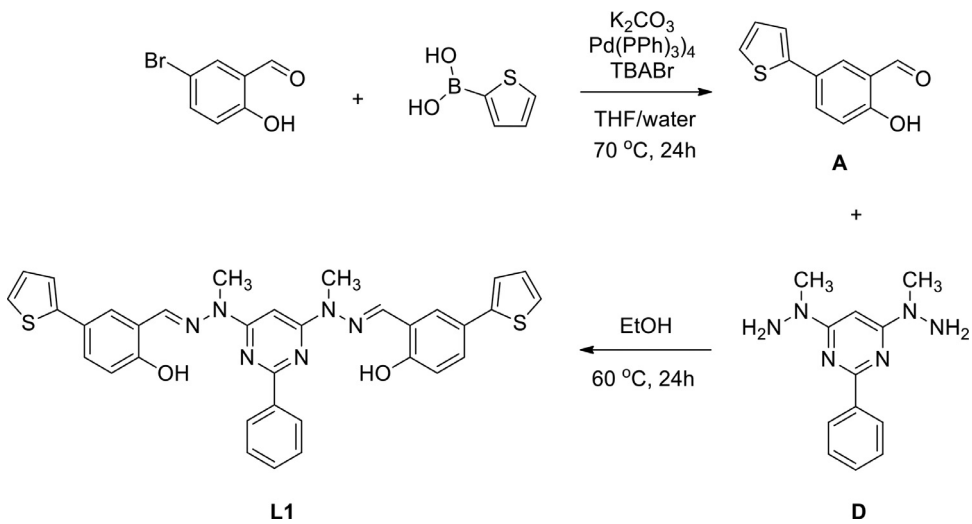

Fig. 2. Synthetic scheme for the preparation of **L1**.

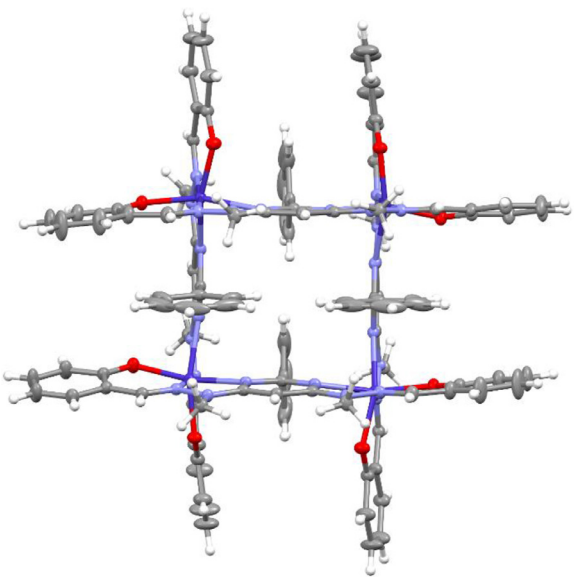

Fig. 3. Anisotropic ellipsoid representation of the complex **2**; ellipsoids are drawn at the 50% probability level, hydrogen atoms are shown as spheres of arbitrary radii.

Table 1
Relevant geometrical data; only three largest angles around Co1 are listed. Symmetry code ^{i} denotes operation 5/4-y,-3/4+x,1/4-z.

Co1-O1	2.0386(13)	Co1-N8	2.1089(16)
Co1-N11	2.2346(15)	Co1-O26^{i}	2.0161(14)
Co1-N23^{i}	2.1094(15)	Co1-N13^{i}	2.2346(15)
N13^{i}-Co1-O26^{i}	157.02(6)	O1-Co1-N11	158.23(5)
N8-Co1-N23^{i}	170.58(6)		

possible to obtain single crystals suitable for X-ray analysis. As it is known that the structure of complexes is dependent on many factors such as type of anion, [58] nature of solvent, [59] presence of oxygen [60] or metal:ligand stoichiometry, [61] ligand **L2** has been used in complexation reaction with the same transition metal salt under exactly the same conditions as **L1**. Single crystal of complex of **L2** with Co(II) **2** suitable for X-ray diffraction analysis has been obtained by the slow diffusion of diethyl ether into the acetonitrile solution of the compound. It was found that ligand **L2** in reactions with $Co(ClO_4)_2$ forms 4:4 metal:ligand complex of grid structure. Fig. 3 shows perspective view of the tetrameric complex **2**, as observed in its crystal structure. The complex molecule is S4-symmetrical, with the four-fold rotoinversion -4 axis running through the middle of the complex. The Co ions are six-coordinated in a distorted octahedral fashion (Table 1 lists the relevant bond lengths and angles).

Cobalt(II) perchlorate has been chosen for complexation reactions due to the fact that perchlorate anion has been found to act as a template in formation of grid-type complexes and cages. [62, 63] The analysis of the crystal structure of complex **2** showed that no perchlorate anions exist in the crystal lattice of **2** (Figure S3). Cobalt(II) ions coordinate with two pyrimidine nitrogen atoms, two nitrogen atoms from imine group and two oxygen atoms from salicylaldehyde group. All OH groups of salicylaldehyde moieties are deprotonated, what leads to formation of neutral Co_4(**L2**-2H)$_4$ supramolecular entities.

The electrochemical properties of grid-type complexes **1** and **2** were measured in three electrode system in degassed and anhydrous 0.1M tetrabutylammonium perchlorate ($TBAClO_4$) in propylene carbonate as a supporting electrolyte. The electrochemical data are summarized in Table 2 and the cyclic voltammograms are presented in Fig. 5A.

It was found that complex **1** exhibits two oxidation/reduction processes at cathodic peak potentials E_{pc} = -550 mV and -1270 mV, and associated with them anodic peak potentials at E_{pa} = -440 mV and -1180 mV respectively. Both of these redox peaks were assigned to the Co(II)/Co(I) reductions of metallic centers in the grid complex. The Co(II)/Co(I) reduction waves of cobalt(II) complex with ligand **L2** were found to be at E_{pc} = -390 mV and -1180 mV, which are 160 mV and 90 mV respectively more positive in comparison to those observed for cobalt(II) complex with ligand **L1**. This is due to the strong electron-donating effect of thiophene ring, [64] which displaces the Co(II)/Co(I) potential waves to more negative values in contrast to electron-withdrawing substituents [65, 66]. The first reduction wave is associated with the oxidation wave at -290 mV and the process was found to be quasi-reversible, while the second reduction is irreversible. No Co(II)/Co(III) oxidation/reduction waves has been observed what can be due to the different self-electron-exchange ability, [67] which has been previously observed for cobalt complexes with terpyridine ligands [24, 68]. The shift of the first reduction potential to less negative value in comparison to Co(II)/Co(I) waves observed for another Co(II) complexes [24, 69]

Table 2
Electrochemical data for Co(II) grids 1 and 2.

Compound	Redox process	E_{pa}	E_{pc}	$E_{1/2}$	ΔE
Complex	$[Co(II)_4]/[Co(II)_2(Co(I))_2]$	-440 mV	-550 mV	-495 mV	110 mV
1	$[Co(II)_2(Co(I))_2]/[Co(I)_4]$	-1180 mV	-1270 mV	-1225 mV	90 mV
Complex	$[Co(II)_4]/[Co(II)_2(Co(I))_2]$	-290 mV	-390 mV	-340 mV	100 mV
2	$[Co(II)_2(Co(I))_2]/[Co(I)_4]$	-	-1180 mV	-	-

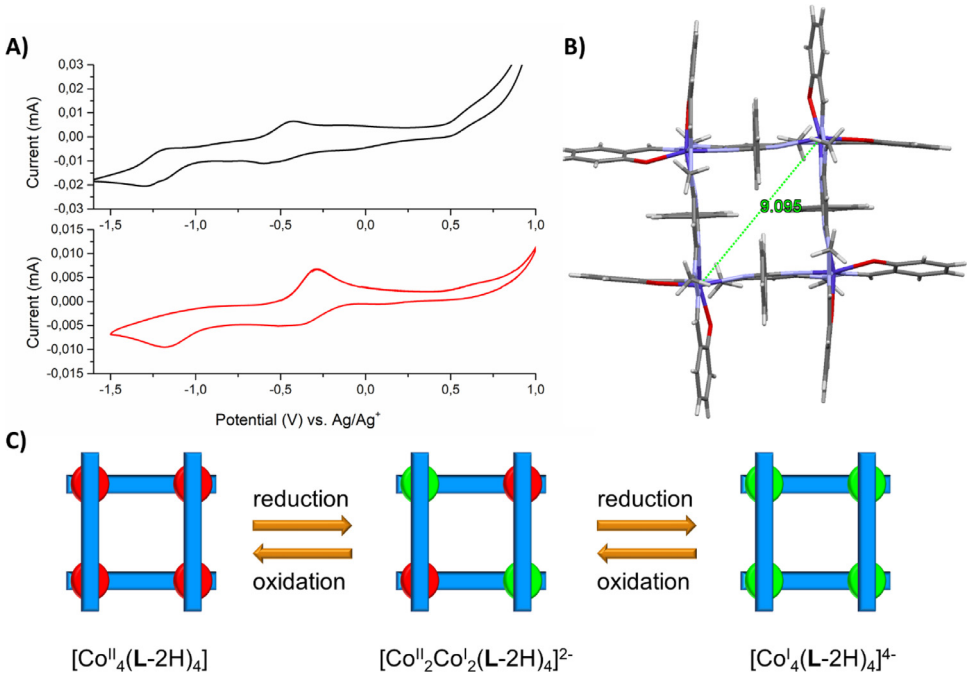

Fig. 4. A) Cyclic voltammetry of cobalt(II) complexes **1** (black) and **2** (red) measured in anhydrous and deaerated 0.1 M $TBAClO_4$ in propylene carbonate as a supporting electrolyte at scan rate 100 mV·s^{-1}. B) Crystal structure of complex **2** showing diagonal distance. C) The scheme showing two-step oxidation/reduction process of grid-type complexes.

was probably caused by the higher number of metallic centers in the complex. Such dependence on oxidation/reduction potential on nuclearity was previously observed for trinuclear Ru(II) complexes [43]. Although it is possible to stepwisely oxidize grid-type complexes with the separation of four oxidation/reduction waves for all metallic centers, [13] in the case of Co(II) grid-type complexes with ligands **L1** and **L2** only two oxidation/reductions peaks have been observed. It is due to the cobalt(II) ions lying diagonally are too far apart to communicate electronically [70]. The distance between two diagonal metal ions was found to be 9.0952(5)Å (Fig. 4B), what is much larger that the distance measured for e.g. iron(II) grid complex with pyrazole-bridged ligand or 2,6-bis(8-quinolylamino)-4-(tert-butyl)phenol (6.291Å) [11, 13]. As a result of this, as shown in Fig. 4C, at first reduction potential two cobalt(II) ions lying diagonally are reduced and at the second reduction potential the reduction of the other two metal ions has been observed. In the consequence these are two-electron processes and the peak separations of 90–110 mV indicate the quasi-reversible character of the processes [71]. When complex **1** was subjected to multiple oxidation/reduction cycles the gradual increase of redox currents at $E_{1/2}$ = -495 mV and -1225 mV (Fig. 5) was observed indicating that the electropolymerization of **1** on the electrode surface occurs and the amount of deposited polymer was increased with successive CV scans. As expected, due to the absence the thiophene rings in complex **2** no electropolymerization was observed.

The mechanism of electropolymerization is similar to those observed for thiophene and its derivatives [72–74]. The monomer is first oxidized by the application of an appropriate oxidation potential, producing the corresponding monomer radical cation (**1**$^{+\bullet}$). The second step involves the coupling of two radical cations to produce a dihydrodimer dication, which after the loss of two protons and rearomatization gives a dimer. Formation of insoluble thin layer of **poly-1** proceeds through successive electrochemical and chemical steps according to a general $E(EC)_n$ mechanism [75].

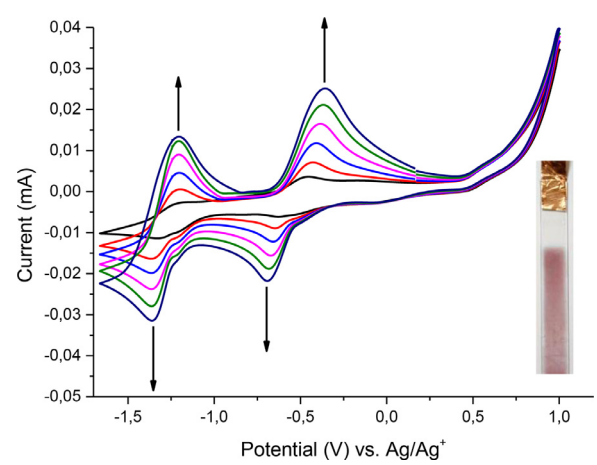

Fig. 5. Cyclic voltammograms of complex **1** in degassed and anhydrous 0.1M solution of $TBAClO_4$ in PC at scan speed 100 mV·s^{-1}. Insert: the picture of ITO glass slide coated with thin film of **poly-1**.

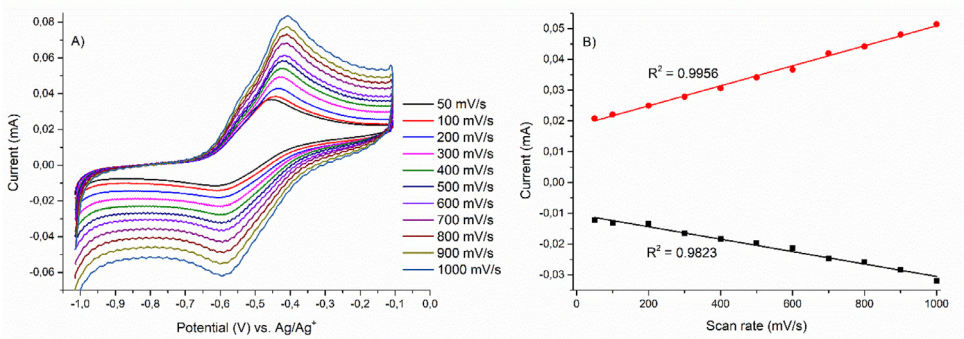

Fig. 6. A) CV profiles of **poly-1** at a different scan rates; B) Linear dependence of the peak currents on the scan rates of the polymeric film of **poly-1**.

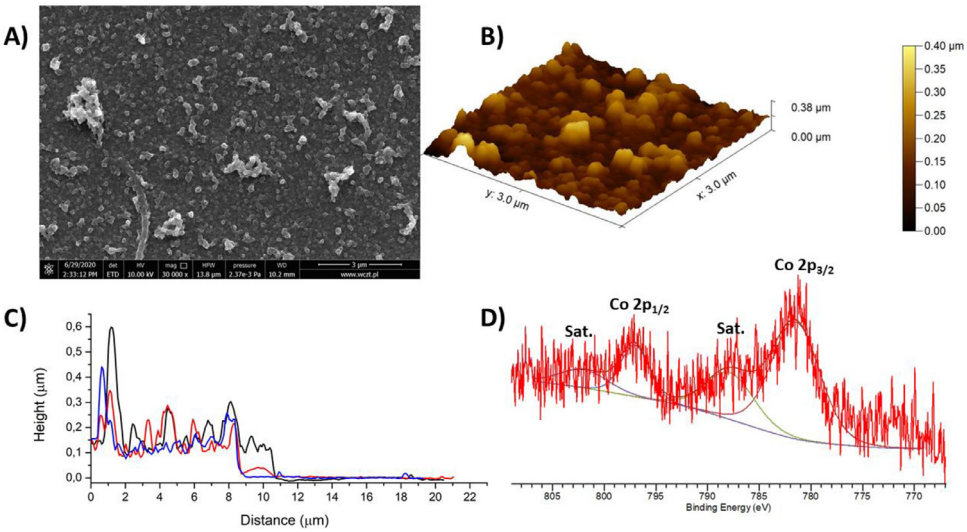

Fig. 7. A) SEM image of thin film of **poly-1** with magnification 3 μm; B) 3D AFM micrograph of **poly-1** deposited on ITO electrode; C) AFM cross-section profiles measured at three different places; D) High-resolution XPS spectra of Co 2p core for **poly-1** sample.

The two-step reduction process of metallic centers has been observed for **poly-1**, what indicates that the basic electrochemical properties of the polynuclear monomer are retained after polymerization [76]. The half-wave potentials of Co(II)/Co(I) waves observed for **poly-1** shifts to more negative values (-525 mV and -1285 mV respectively) in comparison to monomer **1**, what can be due to higher electron donating character of bithiophene substituent [77]. To investigate whether the redox process are controlled by diffusion or adsorption the cyclic voltammograms at a fixed scan rates have been recorded. As seen in Fig. 6 the good linear relationship of i_{pa} and i_{pc} versus the scan speed has been observed for **poly-1** (R^2 = 0.9956 and 0.9823 respectively) indicating that the redox processes are confined on an electrode surface.

In contrast, in case of complex **2** the linear dependence of i_{pa} and i_{pc} versus the square root of scan speed ($v^{1/2}$) (R^2 = 0.9768 and 0.9904, respectively) has been found, which is characteristic of the diffusion-controlled electrochemical events (Figure S4).

The quality of the prepared film was investigated using atomic force microscopy (AFM) and scanning electron microscopy (SEM). These measurements were done to investigate the surface structure of the film and to confirm polymer coverage of the substrate with the electropolymerization method. The AFM topography image was obtained by the scanning of an area of 3 μm x 3μm. The SEM and AFM images are shown in Figs. 7 and S5.

A homogeneous and continuous electrodeposited film of **poly-1** was formed on the substrate. The film is uniform throughout the substrate, with grain sizes below 0.1 μm (Figs. S6 and S7B). The root mean square (RMS) value of the polymer surface was calculated to be 51.66 nm. To measure the average thickness of the film it was cutted with a blade and the difference between bare ITO and polymer surface in three different places (Fig. S7A) was measured using AFM. The measured average film thickness was found to be ~150 nm.

X-ray photoelectron spectroscopy (XPS) was carried out to investigate the composition and chemical oxidation states of cobalt ion in complex **1** and polymer **poly-1**. XPS survey spectra are shown in Figure S8 and they contain peaks of the S 2p, C 1s, N 1s, O 1s and Co 2p core levels. Additionally, the absence of Cl 2p core level confirms that no anions are present in both complex **1** and polymer **poly-1**. The surface molar ratio of Co:N:S in the polymer sample has been calculated to be 1:2.82:1.08 based on the XPS measurement, which is consistent with the composition obtained for complex **1**, where the Co:N:S molar ratio was found to be 1:3.14:1.04. The Co 2p spectrum in Fig. 7D can be deconvoluted into two spin-orbit peaks at the binding energies of 781.48 eV (Co $2p_{3/2}$) and 797.03 eV (Co $2p_{1/2}$), and the corresponding satellite peaks at 787.84 eV and 801.94 eV which are consistent with the presence of Co^{2+} [78].

The ligands and their corresponding Co(II) complexes were investigated using UV-Vis spectroscopy in propylene carbonate solution (Figure S9). The absorption bands in the range 300 nm – 400 nm for ligands **L1** and **L2** and their Co(II) complexes have been assigned to π-π^* transitions, [54] while the shoulders in the ranges 390 nm – 450 nm for complex **2** and 400 nm – 490 nm for complex **1** are MLCT bands [79]. The bathochromic shift of MLCT absorption of **1** in comparison to the MLCT band observed

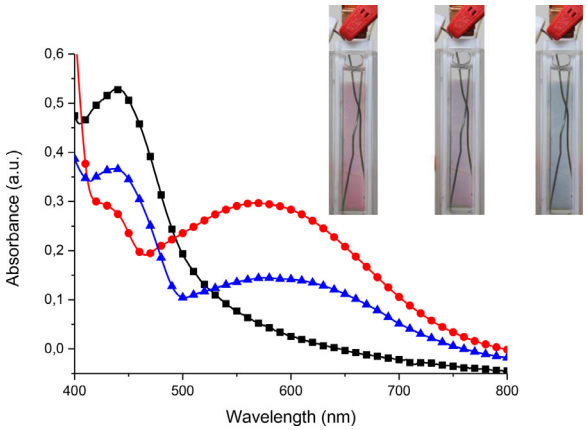

Fig. 8. UV-Vis spectra of **poly-1** with applied potential of 0V (black), -1.0V (blue) and -1.4V (red). Insert: Photographs of **poly-1** with applied voltage of 0V (left) -1.0V (middle) and -1.4V (right).

for complex **2** was due to the increase of conjugation of the ligand molecule [80]. Because the electropolymerization of **1** onto the ITO substrate is efficient enough to observe a purple colored film by the naked eye, the absorption profile of the **poly-1** film was analyzed (Figure S10). It was found that the MLCT peak of **poly-1** was observed at ~442 nm, red-shifted from the MLCT transition of the monomer due to extended conjugation after polymerization [74]. When negative potential was applied to the film the change of the color of the thin film was observed what was spectroscopically tracked using UV-Vis spectroscopy (Fig. 8).

The **poly-1** in its neutral state exhibits MLCT band at ~442 nm. When the negative potential of -1.0V was applied to the film the decrease in the intensity of the MLCT band was observed and simultaneously new absorption band at ~600 nm was formed similarly to those observed for other Co(I) species [24]. This was the result of reduction of poly-[Co^{II}_4(**L2**-2H)$_4$] into poly-[$Co^{II}_2Co^{I}_2$(**L2**-2H)$_4$]$^{2-}$. When potential of -1.4V was applied the reduction into poly-[Co^{I}_4(**L2**-2H)$_4$]$^{4-}$ occurred what resulted in further increase of absorption band at ~600 nm and decrease MLCT band at 442 nm. The film exhibited the color changes from purple via violet to blue based on Co(II)/Co(I) electrochemical process which was similar to this observed for another cobalt(II) complexes. [24, 25, 81]

The obtained thin film of **poly-1** was further examined in terms of its electrochromic properties such as long term stability, switching time, color contrast and coloration efficiency. As it is known that the stability of the thin films increases with the degree of cross-linking, [82, 83] due to the complex contains four thiophene rings it was expected to form highly cross-linked film of good electrochromic stability. The switching characteristics of the film was investigated by chronoamperometry and the corresponding in situ transmittance at 600 nm. The stability of the film was investigated by multiple switching between purple and blue colors by applying potentials of -1.4V and +0.1V in 30 s intervals and the changes in transmittance were monitored at 600 nm (Fig. 9A).

The transmittance difference was 20.7% at the beginning. After 100 oxidation/reduction cycles it decreased to 20.1%, after ~300 oxidation/reduction cycles it dropped down to 16.0% and after ~600 cycles it was found to be 10.7%. Another important criterion for identifying the electrochemical performance of ECDs is the coloration efficiency (CE), which represents the change in the optical density (ΔOD) per unit charge density, which is the change of the charge (Q) consumed per unit electrode area during switching and it can be estimated using following equations:

$$CE = \Delta OD/Q$$

$$\Delta OD = \log(T_b/T_c)$$

where ΔOD is the optical density of the film, Q is the intercalated charge per unit electrode area ($C \cdot cm^{-2}$), T_b and T_c are the values

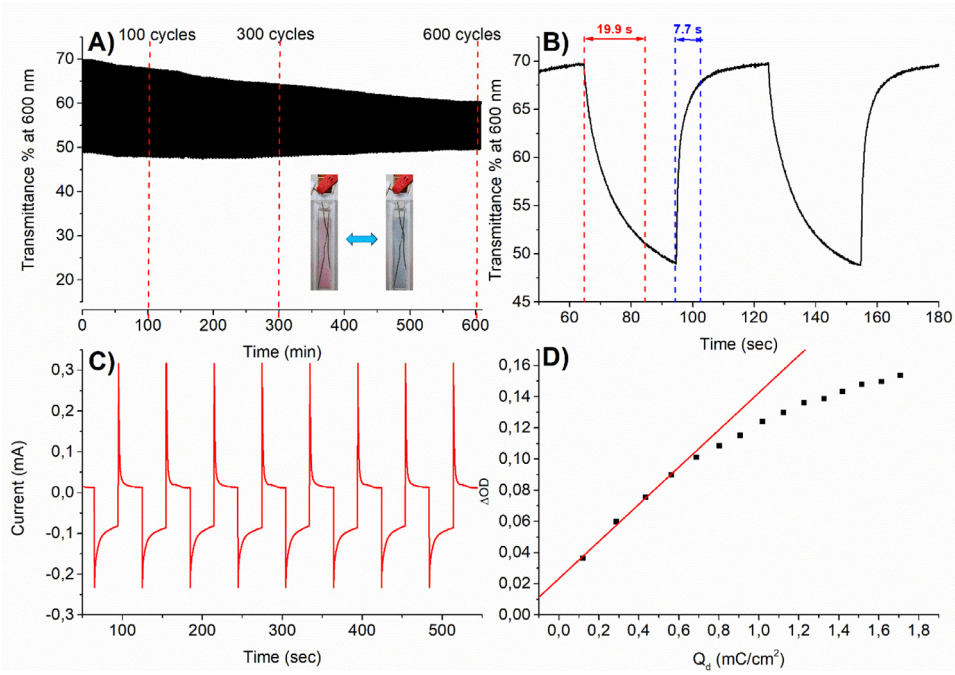

Fig. 9. A) Electrochromic stability of the film of sample 1 of **poly-1** immobilized onto ITO-coated glass slide electrode measured in anhydrous and deaerated 0.1M solution of $TBAClO_4$ in PC by switching between -1.4V and +0.1V in 30 s intervals and monitored at 600 nm. Insert: Photographs of thin film of **poly-1** in its neutral (left) and fully reduced (right) states; B) Coloration and bleaching times of sample 1 of **poly-1**; C) Double potential chronoamperometric study of the switching between -1.4V and +0.1V in 30-s intervals; D) optical density of the **poly-1** at 600 nm versus charge density plot. The CE value was evaluated from the slope of the line fitted to the linear region of the curve (red line) (For interpretation of the references to color in this figure legend, the reader is referred to the web version of this article.).

Table 3
Electrochromic data of samples of **poly-1**.

	ΔT% at 600 nm	ΔT% at 600 nm after 100 cycles	T_c (sec.)	T_b (sec.)
Sample 1	20.7	20.1	19.9 s	7.7 s
Sample 2	20.0	17.8	20.1 s	7.9 s
Sample 3	20.8	20.0	19.2 s	7.6 s
Sample 4	20.45	19.7	19.9 s	7.7 s

of transmittance of the film in its bleached and colored states, respectively. Fig. 9D shows the plot of the in situ optical density at a wavelength of 600 nm versus inserted charge density at a coloration potential of -1.4 V. The CE value is extracted as the slope of the line fitted to the linear region of the curve and it was calculated to be 119.2 cm^2/C.

The coloration time ($T_{c,90}$) and bleaching time ($T_{b,90}$), defined as the time to reach 90% of the final change in transmittance between the steady bleached and colored states [84] were found to be 19.9 s for the coloring and 7.7 s for bleaching processes for sample 1 (Fig. 9B). The long switching times are probably due to slow migration of bulk tetrabutylammonium cations through the polymer layer. To investigate the reproducibility of obtained data the color contrast over 100 switching cycles and switching times were measured for three more samples (Samples 2–4 in Table 3) of **poly-1**. The samples were prepared potentiodynamic method using the same concentration of **1** in the supporting electrolyte and the same parameters of electropolymerization process that were used for preparation of sample 1, what allowed to obtain samples with similar amount of deposited electrochromic material (Figure S11). The electrochromic data of four samples of **poly-1** shown in the Table 3 and Figs. 9 and S12 indicate that the differences in transmittance between two redox states as well as coloring and bleaching times are in case of all prepared samples are similar. This further confirm the reproducibility of obtained results.

4. Conclusion

The two dihydrazone ligands containing two N_2O donor subunits have been synthesized and characterized. The self-assembly of the ligands with cobalt(II) perchlorate lead to obtaining [2 × 2] grid-type complexes $[Co_4(\mathbf{L}\text{-}2H)_4]$. The complexes undergo two-step reduction based on $Co(II)_4/Co(II)_2Co(I)_2$ and $Co(II)_2Co(I)_2/Co(I)_4$ redox processes. The Co(II) complex decorated with four thiophene rings undergoes electropolymerization during multi-scan cyclic voltammetry forming purple, highly cross-linked thin film. The film was found to exhibit three-color electrochromism changing its color from purple via violet to blue due to the stepwise reduction of metallic centers and it exhibits good electrochromic stability during multiple oxidation/reduction cycles, what makes it interesting material for electrochromic applications. In the future, the preparation of the material exhibiting higher number of colors would be possible by the decrease of the distance between diagonal metal ions, what would allow the electronic coupling between them.

Author statement

Sergiusz Napierała: Investigation, **Maciej Kubicki:** Investigation, Writing, Visualization, **Violetta Patroniak:** Writing, Visualization, **Monika Wałęsa-Chorab**: Conceptualization, Methodology, Investigation, Resources, Writing - Review & Editing, Visualization, Supervision, Project administration, Funding acquisition

Declaration of Competing Interest

The authors declare that they have no known competing financial interests or personal relationships that could have appeared to influence the work reported in this paper.

Acknowledgments

We thank Ms. Beata Cichowicz for assistance in synthesis of complex **2**. The financial support received from the National Science Centre, Poland. Grant No 2016/21/D/ST5/01631 are gratefully acknowledged.

Supplementary materials

Supplementary material associated with this article can be found, in the online version, at doi:10.1016/j.electacta.2020.137656.

References

[1] A.-M. Stadler, Grids with unusual, high nuclearity – a structural approach, Eur. J. Inorg. Chem. 2009 (2009) 4751–4770.
[2] M. Ruben, J.-M. Lehn, P. Müller, Addressing metal centres in supramolecular assemblies, Chem. Soc. Rev. 35 (2006) 1056–1067.
[3] M.S. Alam, S. Strömsdörfer, V. Dremov, P. Müller, J. Kortus, M. Ruben, J.-M. Lehn, Addressing the metal centers of [2×2] CoII4 Grid-Type complexes by STM/STS, Angew. Chem. Int. Ed. 44 (2005) 7896–7900.
[4] H. Hofmeier, U.S. Schubert, Recent developments in the supramolecular chemistry of terpyridine–metal complexes, Chem. Soc. Rev. 33 (2004) 373–399.
[5] J.-F. Ayme, J.-M. Lehn, Chapter One - From Coordination Chemistry to Adaptive Chemistry, in: R. van Eldik, R. Puchta (Eds.), Advances in Inorganic Chemistry, Academic Press, 2018, pp. 3–78.
[6] R. Matsuoka, T. Nabeshima, Functional supramolecular architectures of dipyrrin complexes, Front. Chem. 6 (2018).
[7] B. Schäfer, J.-F. Greisch, I. Faus, T. Bodenstein, I. Šalitroš, O. Fuhr, K. Fink, V. Schünemann, M.M. Kappes, M. Ruben, Divergent coordination chemistry: parallel synthesis of [2×2] Iron(II) grid-complex tauto-conformers, Angew. Chem. Int. Ed. 55 (2016) 10881–10885.
[8] V. Patroniak, J.-M. Lehn, M. Kubicki, A. Ciesielski, M. Wałęsa, Chameleonic ligand in self-assembly and synthesis of polymeric manganese(II), and grid-type copper(I) and silver(I) complexes, Polyhedron 25 (2006) 2643–2649.
[9] Z. Yin, S. Wan, J. Yang, M. Kurmoo, M.-H. Zeng, Recent advances in post-synthetic modification of metal–organic frameworks: New types and tandem reactions, Coord. Chem. Rev. 378 (2019) 500–512.
[10] H. Sato, L. Miya, K. Mitsumoto, T. Matsumoto, T. Shiga, G.N. Newton, H. Oshio, Multiredox Active [3 × 3] Copper Grids, Inorg. Chem. 52 (2013) 9714–9716.
[11] N.M. Bonanno, B.O. Patrick, T. Seda, M.T. Lemaire, A Neutral Fe4tBuL4 all ferric grid complex: structural and variable temperature magnetic properties, Eur. J. Inorg. Chem. 2020 (2020) 711–715.
[12] V.C. Lau, L.A. Berben, J.R. Long, [(Cyclen)4Ru4(pz)4]9+: a creutz−taube square, J. Am. Chem. Soc. 124 (2002) 9042–9043.
[13] B. Schneider, S. Demeshko, S. Dechert, F. Meyer, A double-switching multistable Fe4 grid complex with stepwise spin-crossover and redox transitions, Angew. Chem. Int. Ed. 49 (2010) 9274–9277.
[14] M. Steinert, B. Schneider, S. Dechert, S. Demeshko, F. Meyer, Spin-state versatility in a series of Fe4 [2 × 2] grid complexes: effects of counteranions, lattice solvent, and intramolecular cooperativity, Inorg. Chem. 55 (2016) 2363–2373.
[15] J. Tong, S. Demeshko, M. John, S. Dechert, F. Meyer, Redox-induced single–molecule magnetism in mixed-valent [2 × 2] Co4 grid complexes, Inorg. Chem. 55 (2016) 4362–4372.
[16] R.W. Hogue, S. Singh, S. Brooker, Spin crossover in discrete polynuclear iron(ii) complexes, Chem. Soc. Rev. 47 (2018) 7303–7338.
[17] S. Biswas, S. Das, S. Hossain, A.K. Bar, J.-P. Sutter, V. Chandrasekhar, Tetranuclear lanthanide(III) complexes containing a square-grid core: synthesis, structure, and magnetism, Eur. J. Inorg. Chem. 2016 (2016) 4683–4692.
[18] J. Wu, S.-Y. Lin, S. Shen, X.-L. Li, L. Zhao, L. Zhang, J. Tang, Probing the magnetic relaxation and magnetic moment arrangement in a series of Dy4 squares, Dalton Trans 46 (2017) 1577–1584.
[19] R. Banasz, M. Wałęsa-Chorab, Polymeric complexes of transition metal ions as electrochromic materials: synthesis and properties, Coord. Chem. Rev. 389 (2019) 1–18.
[20] J. Zhang, L. Xu, W.-Y. Wong, Energy materials based on metal Schiff base complexes, Coord. Chem. Rev. 355 (2018) 180–198.
[21] B.-B. Cui, J.-H. Tang, J. Yao, Y.-W. Zhong, A molecular platform for multistate near-infrared electrochromism and flip-flop, flip-flap-flop, and ternary memory, Angew. Chem. Int. Ed. 54 (2015) 9192–9197.
[22] B.-B. Cui, C.-J. Yao, J. Yao, Y.-W. Zhong, Electropolymerized films as a molecular platform for volatile memory devices with two near-infrared outputs and long retention time, Chem. Sci. 5 (2014) 932–941.

[23] R. Sakamoto, K. Takada, X. Sun, T. Pal, T. Tsukamoto, E.J.H. Phua, A. Rapakousiou, K. Hoshiko, H. Nishihara, The coordination nanosheet (CONASH), Coord. Chem. Rev. 320-321 (2016) 118–128.
[24] K. Takada, R. Sakamoto, S.-T. Yi, S. Katagiri, T. Kambe, H. Nishihara, Electrochromic Bis(terpyridine)metal complex nanosheets, J. Am. Chem. Soc. 137 (2015) 4681–4689.
[25] D. Arıcan, A. Aktaş, H. Kantekin, A. Koca, Electrochromism of electropolymerized cobaltphthalocyanine–quinoline hybrid, Sol. Energy Mater. Sol. Cells 132 (2015) 289–295.
[26] O. Goktug, T. Soganci, M. Ak, M.K. Sener, Efficient synthesis of EDOT modified ABBB-type unsymmetrical zinc phthalocyanine: optoelectrochromic and glucose sensing properties of its copolymerized film, New J. Chem. 41 (2017) 14080–14087.
[27] M. Wałęsa-Chorab, R. Banasz, D. Marcinkowski, M. Kubicki, V. Patroniak, Electrochromism and electrochemical properties of complexes of transition metal ions with benzimidazole-based ligand, RSC Adv 7 (2017) 50858–50867.
[28] S. Bai, Q. Hu, Q. Zeng, M. Wang, L. Wang, Variations in surface morphologies, properties, and electrochemical responses to nitro-analyte by controlled electropolymerization of Thiophene Derivatives, ACS Appl. Mater. Interfaces 10 (2018) 11319–11327.
[29] S. Cosnier, A. Karyakin, Electropolymerization Concepts, Materials and Applications, Wiley-WCH, 2010.
[30] M. Wałęsa-Chorab, R. Banasz, M. Kubicki, V. Patroniak, Dipyrromethane functionalized monomers as precursors of electrochromic polymers, Electrochim. Acta 258 (2017) 571–581.
[31] T. Yang, C.-X. Zhang, Y.-J. Li, Y.-H. Fu, Z.-H. Yin, L.-H. Gao, K.-Z. Wang, A 3D electropolymerized thin film based on a thiophene-functionalized Ru(ii) complex: electrochemical and photoelectrochemical insights, Inorg. Chem. Front. 6 (2019) 3518–3528.
[32] M. Abe, H. Futagawa, T. Ono, T. Yamada, N. Kimizuka, Y. Hisaeda, An electropolymerized crystalline film incorporating axially-bound metalloporphycenes: remarkable reversibility, reproducibility, and coloration efficiency of ruthenium(II/III)-based electrochromism, Inorg. Chem. 54 (2015) 11061–11063.
[33] T. Schlotthauer, C. Friebe, A.M. Schwenke, M. Jäger, U.S. Schubert, Mild electropolymerization and monitoring of continuous film formation for photoredox-active Ru metallopolymers, J. Mater. Chem. C 5 (2017) 2636–2648.
[34] K. Araki, H. Endo, G. Masuda, T. Ogawa, Bridging Nanogap Electrodes by In Situ Electropolymerization of a Bis(terthiophenylphenanthroline)ruthenium Complex, Chem. Eur. J. 10 (2004) 3331–3340.
[35] A.Et Taouil, J. Husson, L. Guyard, Synthesis and characterization of electrochromic [Ru(terpy)2 selenophene]-based polymer film, J. Electroanal. Chem. 728 (2014) 81–85.
[36] S. Roy, C. Chakraborty, Interfacial coordination nanosheet based on nonconjugated three-arm terpyridine: a highly color-efficient electrochromic material to converge fast switching with long optical memory, ACS Appl. Mater. Interfaces 12 (2020) 35181–35192.
[37] S. Roy, C. Chakraborty, Metallo-macrocycle camouflages: multicolored electrochromism in a Fe(II) based metallo-supramolecular macrocycle utilizing the redox of metal centers and carbazole containing ligand, ACS Appl. Electron. Mater. 1 (2019) 2531–2540.
[38] M.K. Bera, C. Chakraborty, U. Rana, M. Higuchi, Electrochromic Os(II)-based metallo-supramolecular polymers, Macromol. Rapid Commun. 39 (2018) 1800415.
[39] G. Krieger, B. Tieke, Coordinative layer-by-layer assembly of thin films based on metal ion complexes of ligand-substituted polystyrene copolymers and their use as separation membranes, Macromol. Chem. Phys. 218 (2017) 1700052.
[40] M. Anna, R.A. Raman, T. Bernd, Fast-switching electrochromic films of zinc polyiminofluorene-terpyridine prepared upon coordinative supramolecular assembly, Adv. Mater. 21 (2009) 959–963.
[41] E. Puodziukynaite, J.L. Oberst, A.L. Dyer, J.R. Reynolds, Establishing dual electrogenerated chemiluminescence and multicolor electrochromism in functional ionic transition-metal complexes, J. Am. Chem. Soc. 134 (2012) 968–978.
[42] R. Banasz, M. Kubicki, M. Walesa-Chorab, Yellow-to-brown and yellow-to-green electrochromic devices based on complexes of transition metal ions with a triphenylamine-based ligand, Dalton Trans 49 (2020) 15041–15053.
[43] J.-H. Tang, Y.-Q. He, J.-Y. Shao, Z.-L. Gong, Y.-W. Zhong, Multistate redox switching and near-infrared electrochromism based on a star-shaped triruthenium complex with a triarylamine core, Sci. Rep. 6 (2016) 35253.
[44] B.-B. Cui, H.-J. Nie, C.-J. Yao, J.-Y. Shao, S.-H. Wu, Y.-W. Zhong, Reductive electropolymerization of bis-tridentate ruthenium complexes with 5,5′′-divinyl-4′-tolyl-2,2′:6′,2′′-terpyridine, Dalton Trans. 42 (2013) 14125–14133.
[45] J.-Y. Shao, C.-J. Yao, B.-B. Cui, Z.-L. Gong, Y.-W. Zhong, Electropolymerized films of redox-active ruthenium complexes for multistate near-infrared electrochromism, ion sensing, and information storage, Chinese Chem. Lett. 27 (2016) 1105–1114.
[46] M. Nunes, M. Araújo, J. Fonseca, C. Moura, R. Hillman, C. Freire, High-performance electrochromic devices based on Poly [Ni(salen)]-type polymer films, ACS Appl. Mater. Interfaces 8 (2016) 14231–14243.
[47] M. Nunes, C. Moura, A.R. Hillman, C. Freire, Novel hybrid based on a poly [Ni(salen)] film and WO3 nanoparticles with electrochromic properties, Electrochim. Acta 238 (2017) 142–155.
[48] S. Napierała, M. Wałęsa-Chorab, On-substrate postsynthetic metal ion exchange as a tool for tuning electrochromic properties of materials, Eur. Polym. J. 140 (2020) 110052.
[49] M. Lahav, M.E. van der Boom, Polypyridyl metallo-organic assemblies for electrochromic applications, Adv. Mater. 30 (2018) e1706641.
[50] N. Elool Dov, S. Shankar, D. Cohen, T. Bendikov, K. Rechav, L.J.W. Shimon, M. Lahav, M.E. van der Boom, Electrochromic metallo-organic nanoscale films: fabrication, color range, and devices, J. Am. Chem. Soc. 139 (2017) 11471–11481.
[51] CrysAlisPro 1.171.40.53 (Rigaku Oxford Diffraction, 2019).
[52] G. Sheldrick, SHELXT - Integrated space-group and crystal-structure determination, Acta Crystallogr. A 71 (2015) 3–8.
[53] G. Sheldrick, Crystal structure refinement with SHELXL, Acta Crystallogr. C 71 (2015) 3–8.
[54] J. Holub, A. Santoro, J.-M. Lehn, Electronic absorption and emission properties of bishydrazone [2 × 2] metallosupramolecular grid-type architectures, Inorg. Chim. Acta 494 (2019) 223–231.
[55] D.J. Hutchinson, L.R. Hanton, S.C. Moratti, Influence of terminal acryloyl arms on the coordination chemistry of a ditopic pyrimidine–hydrazone ligand: comparison of Pb(II), Zn(II), Cu(II), and Ag(I) Complexes, Inorg. Chem. 52 (2013) 2716–2728.
[56] D.J. Hutchinson, E. Hey-Hawkins, The self-assembly of AgI-containing heterobimetallic complexes with a discriminatory N,P-based heteroditopic ligand, Eur. J. Inorg. Chem. (2018) 4790–4796 2018.
[57] A.R. Stefankiewicz, J. Harrowfield, A.M. Madalan, J.-M. Lehn, Tuning the planarity of [2 × 2] grids, CrystEngComm 15 (2013) 9128.
[58] D. Yang, J. Zhao, X.-J. Yang, B. Wu, Anion-coordination-directed self-assemblies, Org. Chem. Front. 5 (2018) 662–690.
[59] B.-C. Tzeng, H.-T. Yeh, T.-Y. Chang, G.-H. Lee, Novel Coordinated-Solvent Induced Assembly of Cd(II) coordination polymers containing 4,4′-dipyridylsulfide, Cryst. Growth Des. 9 (2009) 2552–2555.
[60] A. Bocian, S. Napierała, A. Gorczyński, M. Kubicki, M. Wałęsa-Chorab, V. Patroniak, The first example of an asymmetrical μ-oxo bridged dinuclear iron complex with a terpyridine ligand, New J. Chem. 43 (2019) 12650–12656.
[61] R.P. Feazell, C.E. Carson, K.K. Klausmeyer, Variability in the Structures of [4-(Aminomethyl)pyridine]silver(I) complexes through effects of ligand ratio, anion, hydrogen bonding, and π-Stacking, Inorg. Chem. 45 (2006) 935–944.
[62] M. Walesa-Chorab, M. Kubicki, M. Korabik, V. Patroniak, Novel self-assembled supramolecular architectures of Mn(ii) ions with a hybrid pyrazine-bipyridine ligand, Dalton Trans 42 (2013) 9746–9754.
[63] R. Vilar, Anion-templated synthesis, Angew. Chem. Int. Ed. 42 (2003) 1460–1477.
[64] S. Zhang, M.U. Ocheje, L. Huang, L. Galuska, Z. Cao, S. Luo, Y.-H. Cheng, D. Ehlenberg, R.B. Goodman, D. Zhou, Y. Liu, Y.-C. Chiu, J.D. Azoulay, S. Rondeau-Gagné, X. Gu, The critical role of electron-donating thiophene groups on the mechanical and thermal properties of donor–acceptor semiconducting polymers, Adv. Electr. Mater. 5 (2019) 1800899.
[65] S. Pizarro, M. Gallardo, F. Gajardo, A. Delgadillo, Electrochemical reduction of lindane using a cobaloxime containing electron-withdrawing groups, Inorg. Chem. Commun. 99 (2019) 164–166.
[66] G. Canard, M. Ponce-Vargas, D. Jacquemin, B.Le Guennic, A. Felouat, M. Rivoal, E. Zaborova, A. D'Aléo, F. Fages, Influence of the electron donor groups on the optical and electrochemical properties of borondifluoride complexes of curcuminoid derivatives: a joint theoretical and experimental study, RSC Adv 7 (2017) 10132–10142.
[67] A.R. Guadalupe, D.A. Usifer, K.T. Potts, H.C. Hurrell, A.E. Mogstad, H.D. Abruna, Novel chemical pathways and charge-transport dynamics of electrodes modified with electropolymerized layers of [Co(v-terpy)2]2+, J. Am. Chem. Soc. 110 (1988) 3462–3466.
[68] C.-Y. Hsu, J. Zhang, T. Sato, S. Moriyama, M. Higuchi, Black-to-transmissive electrochromism with visible-to-near-infrared switching of a Co(II)-based metallo-supramolecular polymer for smart window and digital signage applications, ACS Appl. Mater. Interfaces 7 (2015) 18266–18272.
[69] Y. Liu, R. Sakamoto, C.-L. Ho, H. Nishihara, W.-Y. Wong, Electrochromic triphenylamine-based cobalt(ii) complex nanosheets, J. Mater. Chem. C 7 (2019) 9159–9166.
[70] M. Ruben, E. Breuning, M. Barboiu, J.-P. Gisselbrecht, J.-M. Lehn, Functional Supramolecular Devices: [M4IIL4]8+ [2×2]-Grid-Type Complexes as Multilevel Molecular Electronic Species, Chem. Eur. J. 9 (2003) 291–299.
[71] A.J. Bard, L.R. Faulkner, Electrochemical Methods: Fundamentals and Applications, 2nd Ed., Wiley, 2001.
[72] R.B. Ambade, S.B. Ambade, N.K. Shrestha, R.R. Salunkhe, W. Lee, S.S. Bagde, J.H. Kim, F.J. Stadler, Y. Yamauchi, S.-H. Lee, Controlled growth of polythiophene nanofibers in TiO2 nanotube arrays for supercapacitor applications, J. Mater. Chem. A 5 (2017) 172–180.
[73] C. Li, H. Bai, G. Shi, Conducting polymer nanomaterials: electrosynthesis and applications, Chem. Soc. Rev. 38 (2009) 2397–2409.
[74] Y. Liang, D. Strohecker, V. Lynch, B.J. Holliday, R.A. Jones, A thiophene-containing conductive metallopolymer using an fe(ii) bis(terpyridine) core for electrochromic materials, ACS Appl. Mater. Interfaces 8 (2016) 34568–34580.
[75] S. Sadki, P. Schottland, N. Brodie, G. Sabouraud, The mechanisms of pyrrole electropolymerization, Chem. Soc. Rev. 29 (2000) 283–293.
[76] C.-J. Yao, J. Yao, Y.-W. Zhong, Metallopolymeric films based on a biscyclometalated ruthenium complex bridged by 1,3,6,8-tetra(2-pyridyl)pyrene: applications in near-infrared electrochromic windows, Inorg. Chem. 51 (2012) 6259–6263.
[77] A. Kuhn, K.G. von Eschwege, J. Conradie, Reduction potentials of para-substituted nitrobenzenes—an infrared, nuclear magnetic resonance, and density functional theory study, J. Phys. Org. Chem. 25 (2012) 58–68.

[78] J. Du, G. Liu, F. Li, Y. Zhu, L. Sun, Iron–Salen Complex and Co2+ ion-derived cobalt–iron hydroxide/carbon nanohybrid as an efficient oxygen evolution electrocatalyst, Adv. Sci. 6 (2019) 1900117.
[79] M.A.W. Lawrence, W.H. Mulder, M.J. Celestine, C.D. McMillen, A.A. Holder, Assessment of two cobalt(II) complexes with pincer ligands for the electrocatalytic hydrogen evolution reaction. A comparison of the SNS vs ONS coordination, Inorg. Chim. Acta 506 (2020) 119497.
[80] S. Mukherjee, D.E. Torres, E. Jakubikova, HOMO inversion as a strategy for improving the light-absorption properties of Fe(ii) chromophores, Chem. Sci. 8 (2017) 8115–8126.
[81] M.R.J. Scherer, N.M. Muresan, U. Steiner, E. Reisner, RYB tri-colour electrochromism based on a molecular cobaloxime, Chem. Commun. 49 (2013) 10453–10455.
[82] M. Wałęsa-Chorab, W.G. Skene, Investigation of an electroactive immobilized azomethine for potential electrochromic use, Sol. Energy Mater. Sol. Cells 200 (2019) 109977.
[83] P. Hibon, H. von Seggern, H.R. Tseng, C. Leonhard, M. Hamburger, G. Bealle, Improved thin film stability of differently formulated, printed, and crosslinked polymer layers against successive solvent printing, J. Appl. Polym. Sci. 137 (2020) 48895.
[84] L. Liang, J. Zhang, Y. Zhou, J. Xie, X. Zhang, M. Guan, B. Pan, Y. Xie, High-performance flexible electrochromic device based on facile semiconductor–to-metal transition realized by WO3•2H2O ultrathin nanosheets, Sci. Rep. 3 (2013) 1936.